Overheating risk in Mediterranean residential buildings: Comparison of current and future climate scenarios

Eugénio Rodrigues[a,*], Marco S. Fernandes[a]

[a] *ADAI, LAETA, Department of Mechanical Engineering, University of Coimbra, Rua Luís Reis Santos, Pólo II, 3030-788 Coimbra, Portugal*

Abstract

One of the effects of climate change is global warming, which will increase cooling demand in buildings. However, scientific literature does not show consensus on the risk of highly insulated buildings being prone to overheating. This paper presents a statistical comparison of two synthetic datasets for current and future climates in sixteen Mediterranean locations. The weather data for the 2050 climate projection was generated by 'morphing' current weather data. The buildings were created using a generative design method to produce random geometries and random U-values for the envelope elements. Energy performance was evaluated using dynamic simulation. In addition to the expected general increase in cooling demand (up to 137 %) and a smaller reduction in heating demand (up to 63 %), the results demonstrate that the ideal U-values used in the current climate in almost all of the locations will not cause overheating. In several cases, the decrease of the U-values is even recommended for Podgorica, Valencia, Tunis, Malaga, Larnaca, and Alexandria, as the reduction of heating demand compensates the increase of cooling demand. Casablanca was the only location showing an increase in the ideal U-values, thus presenting risk of overheating if using current ideal U-values.

Keywords: residential buildings, Mediterranean climate, climate change, overheating risk, cooling demand, thermal transmittance

1. Introduction

Despite having less emissions per capita than the actual country's average [1], cities will become substantially warmer in the future [2] due to the growth of the number of urbanites [3] coupled to the warming of the planet [4]. In addition to the adverse impact on human health [5] and the risks associated with poor indoor air quality [6], the rise in average global temperatures also has consequences in the type of energy systems to use [7], as a decrease in heating demand and an increase in cooling consumption is expected [8].

*Corresponding author.
Email address: erodrigues@uc.pt (Eugénio Rodrigues)

A paradigm shift is expected to occur in temperate climates, as new buildings are designed to satisfy cooling needs as opposed to current heating needs. This represents a change in the use of oil- or gas-based systems to electric-based space cooling [9], thus contributing up to 4.6 % in peak electricity demand for each degree of increase in ambient temperature [10]. Since space cooling is expected to have an increasing use of energy, it "induces a vicious circle, being, at the same time, a cause and an effect of the anthropogenic overheating of the planet" [11]. Considering the long lifespan of buildings and the projected effects of climate change scenarios for the 21st century, it is fundamental to understand the energy implications of current design strategies [12].

The consequences of overheating are particularly important in the Mediterranean region (climate region characterized by hot summers and mild winters). Aimed to reduce the energy consumption, the use of low thermal transmittance (U-value) envelope elements (*i.e.*, roof, exterior walls and windows) was legislated to improve passive thermal performance. However, some concerns have arisen from having highly insulated buildings, as these do not consider the risk of overheating in future climate conditions [13]. Therefore, it is fundamental to understand if building envelops with low U-values will not produce undesired effects.

To estimate how buildings will perform in the future, researchers can resort to a top-down or bottom-up approach using projected climate conditions [14]. These climatic projections are obtained from General Circulation Models (GCM) as well as Regional Climate Models (RCM), which have higher spatial resolution than GCM. Both use the emissions scenarios in the form of Representative Concentration Pathways (RCP) as input. GCM are numerical simulations that describe global climate on a global and continental scale, in particular the atmosphere, cryosphere, oceans and land surface, with monthly, seasonal and annual resolutions. As the weather information used by transient building simulations is typically an hourly-based dataset, the current weather time series are morphed by moving the absolute monthly mean ('shift'), by scaling ('stretch'), or by combining both to match different types of variables from the projected climates [15].

There is no consensus in scientific community on the impact of insulation in a climate change scenario. Several studies demonstrate that better insulated buildings will have a positive impact, mainly in reducing heating energy consumption (up to 73 % decrease when combined with efficient glazing), but only a few analyzed the impact on cooling demand [16]. There were still others which found that the overheating risk depends mainly on the capability of the occupants to adapt to the new climate without resorting to air-conditioning [17]. Fosas et al. [18] analyzed the impact of several building variables using a data mining technique to isolate the effect of insulation on overheating. The authors found that insulation accounted for 5 % of overall overheating. Nonetheless, they also determined that in cases where buildings have poor design, the insulation increase is beneficial. Therefore, they recommended that insulation should be part of climate change policies

in cases where the overheating level is acceptable.

Dino and Akgül [19] evaluated the impact of climate change on a residential reference building in several cities in Turkey. The authors found that the increase of ambient temperatures lowered heating consumption and cooling varied in demand according to each climate location. In the warmer locations of Turkey, cooling demand will increase, while in colder climates, mixed-mode buildings will have much lower consumptions than buildings having only cooling air-conditioning. Therefore, the authors conclude that prevention of both overheating and significant increase of cooling energy consumption could be obtained by using natural ventilation and higher cooling setpoints. The authors also state their concern in relation to the combined effect of increased insulation, high summer solar gains, and inefficient daytime cooling. The increase of cooling needs was also predicted for other countries in the Mediterranean, such as Greece [20] and Cyprus [21], the latter having an increase of 6 % in the annual electricity demand in the country.

Moazami et al. [22] determined that peak cooling demand will increase 3.8 % to 13.1 % for apartments in a climate change scenario in Geneva, Switzerland. The authors included future extreme weather conditions in the typical weather datasets, which can empower building engineers and architects to deal with future climate uncertainties. In another study, the decrease of heating needs is shown to be more pronounced in highly insulated buildings and in the coldest locations in Switzerland [23]. However, the same authors found that cooling needs may increase up to 2100 %. These findings are in line with the work of Frank [24] for the same region. The authors point out the need of night ventilation to prevent overheating problems lasting 3 to 9 days in highly insulated buildings.

Pajek and Košir [25] point out that current buildings are mainly designed for passive heating and, therefore, there is a substantial risk of suffering from overheating, as the current bioclimatic design will become irrelevant or extremely inefficient. The authors state that reducing the thermal transmittance of the building envelope might become less important in the future, as the buildings will be characterized by being cooling dependent. Their findings contrast with the ones of Andrić et al. [26], who propose highly insulated envelopes in locations such as Madrid (Spain) and Milan (Italy). Andrić et al. [26] conclusion results from the fact that the impact of climate change is only evaluated with regards to heating demand. The authors' justification to not include total energy consumption is based on the fact that current residential buildings are not equipped with cooling systems; however, this assumption may fail considering that the projection year of the study is 2050 and, as the occupants' thermal comfort needs will increase year-by-year, the purchase of such systems will grow [7]. Similarly, Andrić et al. [27] studied the impact of climate change on heating demand in Alvalade neighborhood, located in Lisbon, Portugal. The level of insulation suggested by the authors varied according to the level of retrofitting, but to reach the NZEB

level, the building envelop elements required a U-value below $0.15\,\mathrm{W}\cdot\mathrm{m}^{-2}\cdot\mathrm{K}^{-1}$. According to Barbosa et al. [28], who also studied the impact of climate change in Lisbon, Portugal, the increase of insulation improved the building's resilience to heat waves (a decrease in 48 % in discomfort hours). However, the study was limited to the cooling season. In contrast, Domínguez-Amarillo et al. [29] found that thermal insulation is a less effective strategy in a climate change scenario for low-income houses located in Seville, Spain.

It is therefore important to include both cooling and heating energy consumptions in the annual assessments, as the cooling-based needs will define a shift in the building design paradigm. Moreover, as cooling systems are essentially electric, the use of photovoltaic systems may minimize consumption of oil- and coal-based primary energy, as future climate scenarios show that these systems can operate for longer hours, as shown by the study carried out by Rey-Hernández et al. [30] in Valladolid, Spain. Pérez-Andreu et al. [31] demonstrated that cooling demand can be reduced if window shades, low infiltration, and natural and mechanical ventilation are used in Valencia, Spain. The authors also found that the change of glazing and window frame had the least impact on energy demand. In addition, Campaniço et al. [32] developed a methodology to assess cooling demand savings by using passive measures, such as direct ventilation and evaporative cooling, in the Iberian Peninsula for the projected climate change 2070-2100.

The literature shows that the common approach is to model the buildings for current weather data, satisfying the maximum allowed U-values according to every national energy code or using the thermophysical proprieties of existing building stock envelopes. The same buildings are then assessed with future climate projections and the increase of insulation levels or lower thermal transmittance values are tested to find the optimum solution. However, this comparison can be misleading as the thermal transmittance values of current weather-evaluated buildings have not have been optimized. Therefore, knowing whether today's highly insulated buildings will be prone to overheating should result from comparing the ideal U-values for current and future weather scenarios. If the ideal U-values are higher for future scenario, then the increased insulation will have the undesired effect of overheating. However, if ideal U-values are lower, then no risk is associated.

This paper compares the energy performance of buildings from two synthetic datasets with random building geometries and random thermal transmittance values for sixteen locations in the Mediterranean region. Both current weather data and projected climate change scenario for 2050 are used. The buildings were produced using a generative design method and evaluated using dynamic simulation. Finally, a statistical analysis was carried out to identify the ideal U-values for each location and climate scenario. A comparison between both datasets was carried out to determine the impact of climate change in the Mediterranean region.

2. Methodology

The methodology of this study consists of five phases. In the first phase, sixteen locations in the Mediterranean region are chosen and the current reference weather data gathered. The locations were chosen to represent the entire Mediterranean zone. In the second phase, the gathered weather data are morphed for the 2050 climate change projection using the CCWorldWeatherGen software [33]. In the following phase, buildings are created using the Evolutionary Program for the Space Allocation Problem (EPSAP) [34] with random geometries and random thermal transmittance values for the opaque and transparent envelope elements. The energy consumption for air-conditioning for every building is then evaluated [35, 36] for every location, using the coupled dynamic simulation engine EnergyPlus [37]. For the purpose of comparison, the specifications for locations, buildings' layout, construction system, occupancy, lighting, internal gains and HVAC are the same as in Ref. [38]. Finally, in the fifth phase, a statistical comparison analysis is carried out to determine if the ideal U-values for 2050 climate projection are different from the values for the current weather data. The study concept framework is illustrated in Fig. 1.

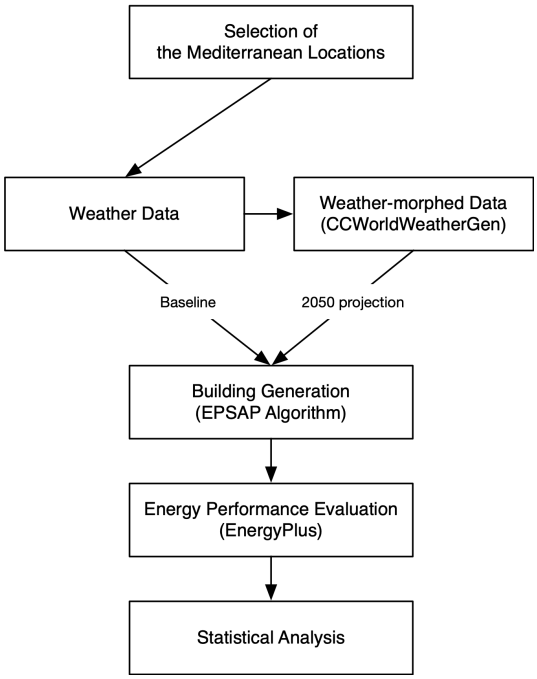

Fig. 1. Study concept framework.

2.1. Locations and weather data

Sixteen locations were chosen in the Mediterranean region (sorted by latitude): Venice (Italy, ITA), Marseille (France, FRA), Podgorica (Montenegro, MNE), Istanbul (Turkey, TUR), Naples (ITA), Valencia (Spain, ESP), Izmir (TUR), Athens (Greece, GRC), Tunis (Tunisia, TUN), Algiers (Algeria, DZA), Malaga (ESP), Larnaca (Cyprus, CYP), Casablanca (Morocco, MAR), Tripoli

(Libya, LBY), Tel Aviv (Israel, ISR), and Alexandria (Egypt, EGY). Fig. 2 maps every chosen location.

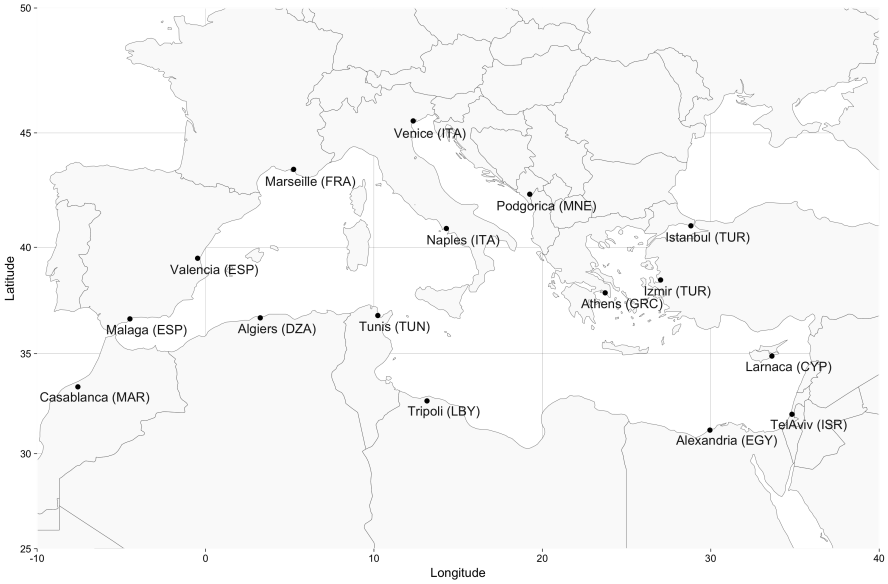

Fig. 2. Map of the studied locations in the Mediterranean [38].

According to the Köppen-Geiger World Map climate classification [39], the locations are characterized as being humid subtropical (mild with no dry season and hot summer), except for Malaga (ESP), which has a Mediterranean climate (dry hot summer and mild winter), and Tripoli (LBY), which is classified as a hot subtropical steppe. With the exception of Malaga (ESP), Tel Aviv (ISR), and Alexandria (EGY), the weather data type for all remaining locations is International Weather for Energy Calculations (IWEC), which is derived from DATSAV3 hourly weather data, ranging from 1982 to 1999. The weather data for Malaga (ESP) was synthetically generated from mean monthly data obtained from the Spanish Meteorological National Institute, gathered between 1960 and 1990 (Spanish Weather for Energy Calculations, SWEC). The wind speeds in SWEC present a constant value of $6.7\,\mathrm{m}\cdot\mathrm{s}^{-1}$. The weather data for Alexandria (EGY) was developed from data provided by the US National Climatic Data Center, recorded between 1982 and 2003 (Egyptian Typical Meteorological Year, ETMY). Lastly, the weather data for Tel Aviv (ISR) was obtained from the Israel Meteorological Service (IMS). Since Tel Aviv (ISR) weather data could not be morphed for a future climate change scenario due to the lack of certain solar radiation-related variables, the morphed weather data was derived from the ISD-TMYx (US NOAA's Integrated Surface Database) with hourly data from 2008 to 2017 (in this case, the rise of temperature may be overestimated due to the reference years being from the last decade). All baseline weather files may be obtained from the EnergyPlus website [37] and the weather data used to project the climate change for Tel Aviv (ISR) was obtained from Climate.OneBuilding.Org website [40]. Table 1 summarizes the geographical and climatic information of each location.

Table 1. Climate classification of each location [38].

Location					Climate		
City	Country	Lat. (°)	Long. (°)	Alt. (m)	Type	Climate description	Data type
Venice	Italy (ITA)	45.50 N	12.33 E	6	Cfa	Humid subtropical (mild with no dry season, hot summer)	IWEC
Marseille	France (FRA)	43.45 N	5.23 E	36	Cfa	Humid subtropical (mild with no dry season, hot summer)	IWEC
Podgorica	Montenegro (MNE)	42.37 N	19.25 E	33	Cfa	Humid subtropical (mild with no dry season, hot summer)	IWEC
Istanbul	Turkey (TUR)	40.97 N	28.82 E	37	Cfa	Humid subtropical (mild with no dry season, hot summer)	IWEC
Naples	Italy (ITA)	40.85 N	14.30 E	72	Cfa	Humid subtropical (mild with no dry season, hot summer)	IWEC
Valencia	Spain (ESP)	39.50 N	0.47 W	62	Cfa	Humid subtropical (mild with no dry season, hot summer)	IWEC
Izmir	Turkey (TUR)	38.50 N	27.02 E	5	Cfa	Humid subtropical (mild with no dry season, hot summer)	IWEC
Athens	Greece (GRC)	37.90 N	23.73 E	15	Cfa	Humid subtropical (mild with no dry season, hot summer)	IWEC
Tunis	Tunisia (TUN)	36.83 N	10.23 E	4	Cfa	Humid subtropical (mild with no dry season, hot summer)	IWEC
Algiers	Algeria (DZA)	36.72 N	3.25 E	25	Cfa	Humid subtropical (mild with no dry season, hot summer)	IWEC
Malaga	Spain (ESP)	36.67 N	4.49 W	7	Csa	Mediterranean climate (dry hot summer, mild winter)	SWEC
Larnaca	Cyprus (CYP)	34.88 N	33.63 E	2	Cfa	Humid subtropical (mild with no dry season, hot summer)	IWEC
Casablanca	Morocco (MAR)	33.37 N	7.58 W	206	Cfa	Humid subtropical (mild with no dry season, hot summer)	IWEC
Tripoli	Libya (LBY)	32.67 N	13.15 E	81	BSh	Hot subtropical steppe	IWEC
Tel Aviv	Israel (ISR)	32.00 N	34.82 E	35	Cfa	Humid subtropical (mild with no dry season, hot summer)	IMS
Alexandria	Egypt (EGY)	31.20 N	29.95 E	7	Cfa	Humid subtropical (mild with no dry season, hot summer)	ETMY

For each location, the future climate was statistically morphed using the CCWorldWeatherGen software (version 1.9) [33], according to the GCM from the Hadley Centre Coupled Model, version 3 (HadCM3), and the selected A2 scenario, which represents the business as usual of medium-high emissions [41]. In the monthly resolution for each grid point of the 1961-1990 baseline climate, the data for HadCM3 A2 experiments include the total downward shortwave flux, the total cloud in longwave radiation, the precipitation rate, the mean temperature, the daily minimum temperature, the daily maximum temperature, the relative humidity, the mean sea level pressure, and the wind speed (each parameter is averaged from the three experiment runs). The parameters of the nearest four grid points of the chosen weather station are combined. The weather station parameters are morphed for one of the three time slices of 2020, 2050, and 2080 (see Refs. [42, 43] for the complete list of parameters and used techniques). In this work, only the projected climate for the time slice of 2050 was used. The 2020 projection was considered too proximate to the current day, thus limited in application, while the 2080 involves several social, economic, and technologic uncertainties that reduce the confidence in the results.

2.2. Building generation

The Evolutionary Program for the Space Allocation Problem (EPSAP) algorithm [34] was used to generate alternative building geometries that satisfy the same initial preferences and requirements. The indoor floor plan layout in each story is created according to the geometric and topologic specifications for each space and opening. The algorithm produces a user specified number of solutions by satisfying all specifications in an evolution strategy approach, where the traditional mutation operator is replaced by transformation operations that perform geometric actions, such as translation, rotation, stretching, mirroring, etc. The algorithm minimizes a weighted-sum cost function of seventeen penalty functions that evaluate the layout gross and construction areas, story gross area, floor plan compactness, floor plan overflow, circulation space area, space connectivity,

overlapping, fixed position, dimensions and relative importance, opening accessibility, as well as dimensions, overlapping, orientation, and fixed position of openings (the complete description of the algorithm can be found in Ref. [34]).

In this study, the building specifications correspond to a two-story family house comprising a hall, a living room, a kitchen, and a bathroom on the ground floor level; a corridor, a master bedroom, a double bedroom, a single bedroom, and a second bathroom on the upper floor, with a staircase connecting both levels (see Table 2). The geometry specifications for each space are presented in Table 2, including type (circulation, service, or living), relative importance (ranks the importance of each space in comparison to the remaining spaces from none to max), associated stories, minimum space floor side dimension, minimum space floor area, and ratios for the space floor sides. The geometry specifications for the exterior openings in each space are presented in Table 3: opening type (door, gate, or window), minimum width, minimum height, and relative vertical position of the opening to the story floor level. The geometry specifications for interior openings are presented in Table 4, for which their adjacency relations between contiguous spaces is also specified. Examples of the generated buildings are presented in Fig. 3.

Table 2. Geometry specifications for the different spaces [38].

Space	C^{sn}	C^{sf}	C^{ri}	C^{sl}	C^{su}	C^{ss} (m)	C^{sa} (m^2)	C^{ssr}	C^{slr}
S_1	Hall	Circulation	Min	L_1	L_1	2.70	10.0	{2.0, 3.0}	{3.0, 1.5}
S_2	Living room	Living	Max	L_1	L_1	3.20	–	1.7	2.0
S_3	Kitchen	Service	Mid	L_1	L_1	1.80	–	1.7	2.0
S_4	Bathroom	Service	Min	L_1	L_1	2.20	–	1.7	2.0
S_5	Stair	Circulation	–	L_1	L_2	–	–	–	–
S_6	Corridor	Circulation	None	L_2	L_2	1.40	6.0	{2.0, 3.0}	{3.0, 1.5}
S_7	Double bedroom	Living	High	L_2	L_2	2.70	–	1.7	2.0
S_8	Main bedroom	Living	High	L_2	L_2	2.70	–	1.7	2.0
S_9	Single bedroom	Living	Mid	L_2	L_2	2.70	–	1.7	2.0
S_{10}	Bathroom	Service	Min	L_2	L_2	2.20	–	1.7	2.0

C^{sn} – name, C^{sf} – function, C^{ri} – relative importance, C^{sl} and C^{su} – served lower and upper stories, C^{ss} – minimum side, C^{sa} – minimum area, C^{ssr} and C^{slr} – space small side and large side ratios

Table 3. Geometry specifications for exterior openings [38].

C^{os}	Opening	C^{oet}	C^{oew} (m)	C^{oeh} (m)	C^{oev} (m)
S_1	Oe_1	Door	1.00	2.00	0
S_2	Oe_2	Window	2.80	2.00	0
S_3	Oe_3	Window	1.20	1.00	1.00
S_4	Oe_4	Window	0.60	0.60	1.40
S_5	Oe_5	Window	0.80	1.40	0.80
S_6	–	–	–	–	–
S_7	Oe_6	Window	1.80	1.00	1.00
S_8	Oe_7	Window	1.80	1.00	1.00
S_9	Oe_8	Window	1.20	1.00	1.00
S_{10}	–	–	–	–	–

C^{os} – space, C^{oet} – opening type, C^{oew} – minimum width, C^{oeh} – minimum height, C^{oev} – vertical position

2.3. Building evaluation

After each EPSAP algorithm run, the building's performance evaluation was carried out using the coupled dynamic simulation engine EnergyPlus [35, 36]. EnergyPlus software was used for

Table 4. Geometry and topologic specifications for interior openings [38].

Opening	C^{oit}	C^{oia}	C^{oib}	C^{oiw} (m)	C^{oih} (m)	C^{oiv} (m)
Oi_1	Door	S_1	S_2	1.40	2.00	0
Oi_2	Door	S_1	S_3	0.90	2.00	0
Oi_3	Door	S_1	S_4	0.90	2.00	0
Oi_4	Door	S_5	S_1	0.90	2.00	0
Oi_5	Adjacency	S_2	S_3	0	–	–
Oi_6	Door	S_5	S_6	0.90	2.00	0
Oi_7	Door	S_6	S_7	0.90	2.00	0
Oi_8	Door	S_6	S_8	0.90	2.00	0
Oi_9	Door	S_6	S_9	0.90	2.00	0
Oi_{10}	Door	S_6	S_{10}	0.90	2.00	0

C^{oit} – type, C^{oia} – opening's space, C^{oib} – destination space,
C^{oiw} – minimum width, C^{oih} – minimum height, C^{oiv} – vertical position

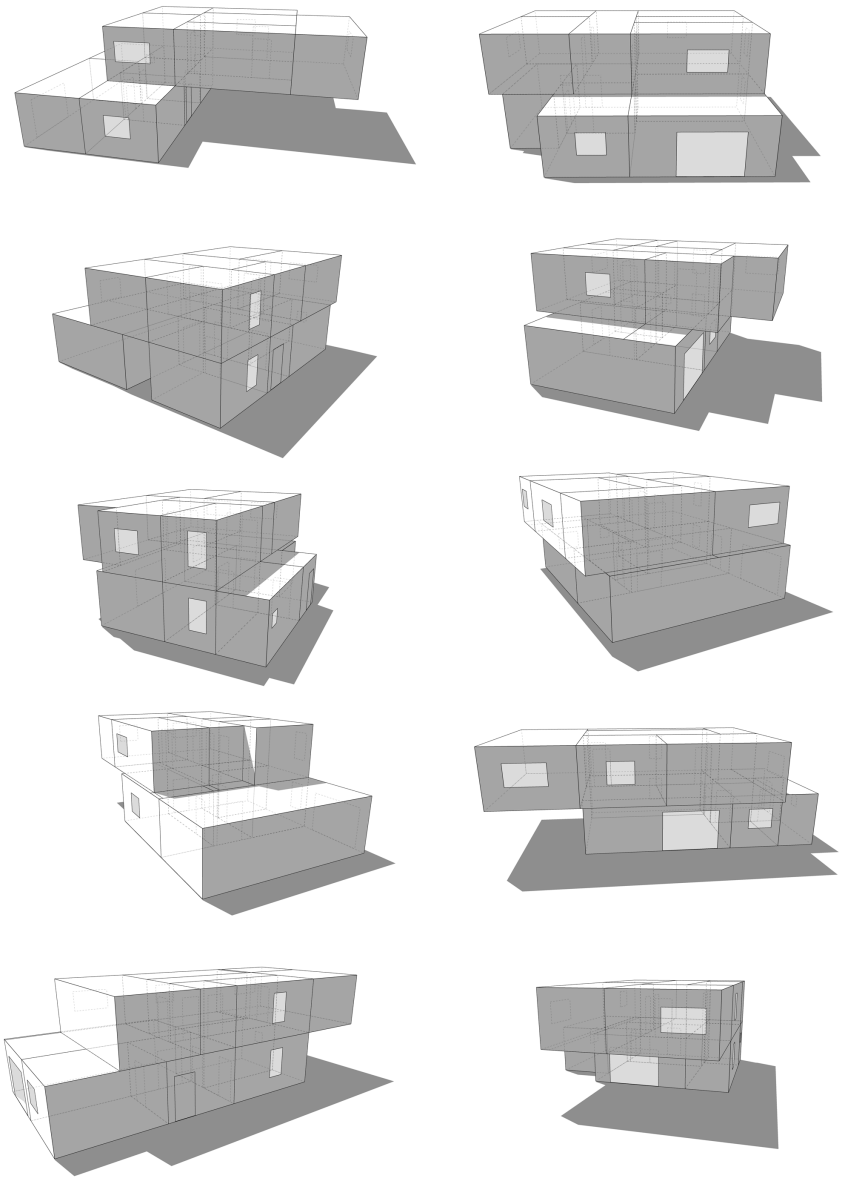

Fig. 3. Examples of buildings generated by the algorithm EPSAP.

a detailed multi-zone energy performance assessment, considering a yearly period. The selected time step for simulation was 15 min. The geometric input requirements are related to each EPSAP

algorithm run, as referred in Rodrigues et al. [34], while the construction, internal thermal gains and HVAC input specifications are described below. In the scope of this work, the outputs are mainly related to the thermal energy demand; *i.e.*, the total, heating and cooling energy consumptions for each one of the buildings' zones.

2.3.1. Occupancy, lighting, internal gains, and HVAC

The building is a single-family dwelling with an occupancy of 5 people. The occupancy patterns and activity levels are presented in Table 5 and Fig. 4, and are based on the building typology.

Table 5. Maximum number of people per zone and correspondent activity levels [38].

Zone type	**Max number of people**[a]	**Activity level** ($W \cdot person^{-1}$)
Living room	5	110
Bathrooms	1	207
Circulation areas	1	190
Kitchen	2	190
Double/Main bedroom	2	72
Single bedroom	1	72

[a] – Regarding the building inhabitants accessing each zone, and not necessarily the number of occupants simultaneously in the zone. The occupant's distribution is defined together with the proper occupancy schedules.

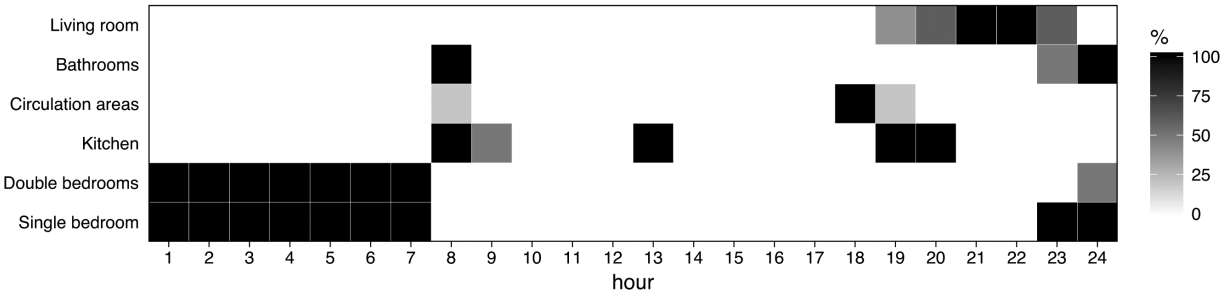

Fig. 4. General occupancy pattern in the building zones [38].

The lighting design levels and schedules are presented in Table 6 and Fig. 5, and are based on the building's zone typology and occupancy, and on the window shading profiles. The window shadings are PVC roller shutters that cover all windows during night-time. Furthermore, daylighting controls dim the light intensity in spaces with exterior windows, switching them off when daylight illuminance is above 300 lx. This dimming control is a 'simulation procedure' that allows to adjust the lighting values according to available daylight in each latitude, since the electric lighting profiles are identical in all locations. The equipment design levels and schedules are presented in Table 7 and Fig. 6, and are also based on the building's zone typology and occupancy.

Cooling and heating are only considered in the living room and the bedrooms. The ideal loads air system model of EnergyPlus is used [44], with the heating/cooling availability schedule for each space defined by the respective occupancy pattern (Fig. 4). The temperature thermostat setpoints for cooling and heating are 25.0 °C and 20.0 °C, respectively, for all the case studies. Mechanical

Table 6. Maximum design lighting levels for each zone type [38].

Zone type	**Design lighting level** ($\mathrm{W \cdot m^{-2}}$)
Living room/Bedrooms	7.5
Bathrooms	7.5
Circulation areas	3.2
Kitchen	5

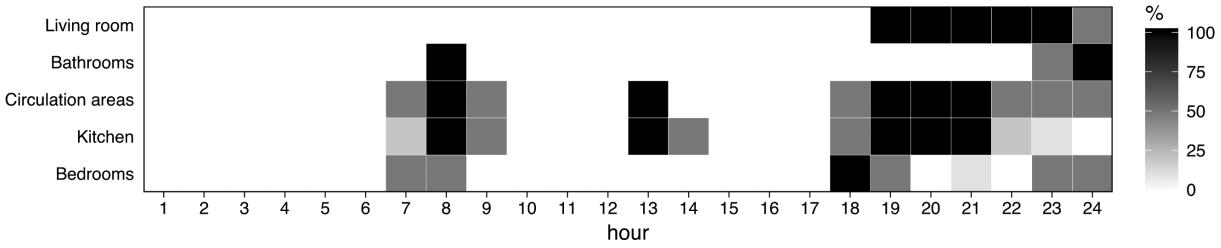

Fig. 5. Electric light schedule in each zone.

Table 7. Total heat gains from electric equipment in each zone.

Zone type	**Design level** (W)
Living room	350
Bathrooms	100
Circulation areas	20
Kitchen	1440
Bedrooms	250

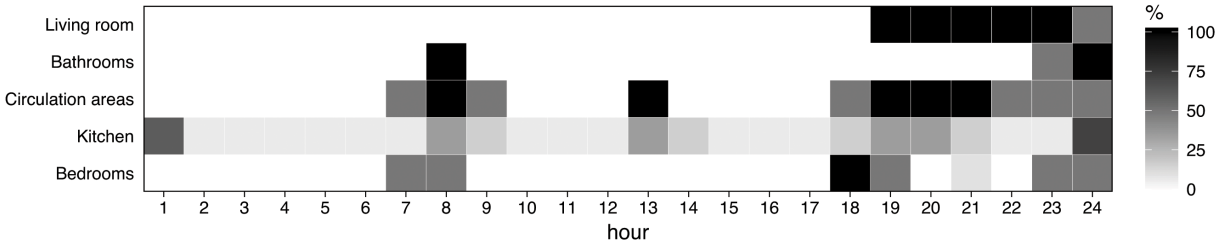

Fig. 6. Electric equipment schedules in each zone [38].

ventilation is considered in the kitchen and bathrooms with a 0.6 air changes per hour (ACH) exhaust rate and a profile equivalent to the occupancy schedules defined for these spaces (Fig. 4). In addition, 0.2 ACH and 0.1 ACH are considered for the outdoor air infiltration into zones with and without exterior openings, respectively.

2.3.2. Construction system

The building's construction elements and respective properties are presented in Table 8. The thermal mass of exterior walls, roofs and suspended slabs is equivalent to that of the interior slab (see Table 8), while their U-value is randomly changed throughout the dynamic simulations – $0.05\,\mathrm{W \cdot m^{-2} \cdot K^{-1}}$ to $1.25\,\mathrm{W \cdot m^{-2} \cdot K^{-1}}$, in steps of $0.05\,\mathrm{W \cdot m^{-2} \cdot K^{-1}}$. The same U-values are also applied to exterior doors. Overall, the building presents a high thermal mass. Regarding the exterior windows, the variable U-values are proportionally paired with those of the opaque elements – $0.2\,\mathrm{W \cdot m^{-2} \cdot K^{-1}}$ to $5.0\,\mathrm{W \cdot m^{-2} \cdot K^{-1}}$, in steps of $0.2\,\mathrm{W \cdot m^{-2} \cdot K^{-1}}$. This pairing

follows the tendency of real cases, where the U-values of both opaque and transparent elements tend to decrease or increase proportionally, allowing to transversally compare the studied locations without interference from local specificities that result from legislation, culture and construction material. In addition, a constant solar heat gain coefficient (SHGC) of 0.6 is considered.

Table 8. Building elements thermophysical properties [38].

Element	**Layer**	**Thick.** (m)	k ($\mathrm{W \cdot m^{-1} \cdot K^{-1}}$)	ρ ($\mathrm{kg \cdot m^{-3}}$)	c_p ($\mathrm{J \cdot kg^{-1} \cdot K^{-1}}$)	U ($\mathrm{W \cdot m^{-2} \cdot K^{-1}}$)	**Mass** ($\mathrm{kg \cdot m^{-2}}$)	**SHGC**
Ground floor	Structural layer	0.2	1.73	2245.6	836.8	0.437	509.69	–
	Insulation layer	0.08	0.04	32.1	836.8			
	filling layer	0.02	0.8	1600	840			
	Regulation layer	0.01	0.22	950	840			
	finishing layer	0.02	0.2	825	2385			
Interior door	finishing layer	0.005	0.2	825	2385	2.009	21.15	–
	Structural layer	0.03	0.067	430	1260			
	finishing layer	0.005	0.2	825	2385			
Interior wall	finishing layer	0.02	0.22	950	840	4.499	195.01	–
	Structural layer	0.07	1.73	2243	836.8			
	finishing layer	0.02	0.22	950	840			
Interior slab	finishing layer	0.02	0.22	950	840	2.841	494.12	–
	Structural layer	0.2	1.73	2245.6	836.8			
	Regulation layer	0.01	0.22	950	840			
	finishing layer	0.02	0.2	825	2385			
Envelope	Thermal mass equivalent to the interior slab					RAND{0.05, ⋯, 1.25}	–	–
Exterior window	–					RAND{0.2, ⋯, 5.0}	–	0.6

k – thermal conductivity, ρ – density, c_p – specific heat, U – thermal transmittance, SHGC – solar heat gain coefficient

2.4. Comparison analysis

For the baseline and the 2050 climate projection, a synthetic dataset was created with the buildings' geometry data (number of stories, spaces, openings, elements surface areas, volumes, and other geometric information), construction data (transparent and opaque elements physical properties), and performance data (electric energy consumption, water consumption, thermal discomfort, and thermal energy production). Each dataset totalizes 192 000 dwellings; *i.e.*, 12 000 buildings per location. These two datasets are publicly available online (see Ref. [45] for baseline and Ref. [46] for 2050 climate projection).

With these two datasets, a graphical comparison and statistical analysis was conducted by splitting each one into groups by their location and into subgroups according to the thermal transmittance values of their envelope elements. The total energy consumption average for air-conditioning, the standard deviation (σ), and the differences of total energy, cooling energy, and heating energy between the baseline and the 2050 climate projection for each of the subgroup were calculated. The subgroup with the lowest total energy consumption average was determined to find the ideal U-values for transparent and opaque elements in each Mediterranean location.

3. Results and Discussion

The results of the morphing procedure are presented in Table 9. Except for Tel Aviv (ISR), the average dry-bulb temperature difference between the baseline and the 2050 projection varies in all

locations from 1.8 °C to 2.9 °C. In what regards relative humidity, the average difference varies from −6.0 % to 0.2 %. Venice (ITA), Podgorica (MNE), and Malaga (ESP) present the highest relative humidity reduction, while Naples (ITA) presents a slight increase. The global horizontal radiation average difference ranges from $-1.9\,\mathrm{W\cdot h\cdot m^{-1}}$ to $10.4\,\mathrm{W\cdot h\cdot m^{-1}}$. Podgorica presents the highest increase and Larnaca (CYP), Casablanca (MAR) and Alexandria (EGY) show a decrease. The average wind speed difference varies from $-0.1\,\mathrm{m\cdot s^{-1}}$ to $0.2\,\mathrm{m\cdot s^{-1}}$. Relatively to Tel Aviv, the average difference of some of the parameters is noticeably higher than in the remaining locations. This is due to the use of weather data from the period 2008-2017, which overestimates the effects of climate change.

Table 9. Climate data comparison between baseline and the 2050 projected climate for each location.

Location	**Climate**	**Dry-bulb temperature** (°C)		**Relative humidity** (%)		**Global hor. rad.** ($\mathrm{W\cdot h\cdot m^{-1}}$)		**Wind speed** ($\mathrm{m\cdot s^{-1}}$)	
		avg.	dif.	avg.	dif.	avg.	dif.	avg.	dif.
Venice (ITA)	Baseline	13.24	2.92	76.93	-5.95	131.66	8.68	1.89	0.06
	2050	16.17		70.99		140.35		1.96	
Marseille (FRA)	Baseline	14.83	2.22	69.19	-3.42	176.41	8.53	4.96	0.01
	2050	17.05		65.77		184.95		4.98	
Podgorica (MNE)	Baseline	15.15	2.80	66.75	-5.36	186.38	10.39	2.57	0.07
	2050	17.95		61.39		196.77		2.64	
Istanbul (TUR)	Baseline	14.50	2.74	72.18	-4.02	159.12	6.86	4.76	0.15
	2050	17.24		68.17		165.97		4.91	
Naples (ITA)	Baseline	16.33	1.78	72.44	0.16	167.86	6.09	2.60	0
	2050	18.12		72.60		173.95		2.60	
Valencia (ESP)	Baseline	17.30	2.43	68.38	-4.02	186.30	6.77	3.56	0.01
	2050	19.73		64.36		193.07		3.57	
Izmir (TUR)	Baseline	16.73	2.52	65.01	-3.26	192.82	4.94	4.38	0.10
	2050	19.25		61.76		197.76		4.49	
Athens (GRC)	Baseline	17.90	2.20	61.52	-1.83	190.59	5.22	3.18	0.01
	2050	20.10		59.69		195.82		3.19	
Tunis (TUN)	Baseline	18.80	1.90	71.56	-0.92	193.83	2.58	4.27	-0.10
	2050	20.70		70.64		196.40		4.17	
Algiers (DZA)	Baseline	17.68	1.90	75.26	-1.10	192.12	1.13	3.02	0.01
	2050	19.58		74.16		193.26		3.03	
Malaga (ESP)	Baseline	17.99	2.86	66.04	-6.02	201.53	7.16	6.70	0.09
	2050	20.85		60.01		208.69		6.79	
Larnaca (CYP)	Baseline	19.37	1.90	68.55	-0.65	213.76	-1.88	3.62	-0.03
	2050	21.27		67.91		211.88		3.59	
Casablanca (MAR)	Baseline	17.32	2.09	75.27	-1.50	205.23	-0.35	3.34	0.01
	2050	19.41		73.78		204.87		3.35	
Tripoli (LBY)	Baseline	20.35	1.83	66.55	-0.35	212.81	1.80	3.70	-0.08
	2050	22.18		66.20		214.61		3.62	
Tel Aviv (ISR)	Baseline	18.96	4.13	70.97	-4.08	213.97	20.47	2.99	-0.38
	2050	23.09		66.89		234.44		2.61	
Alexandria (EGY)	Baseline	20.41	2.04	69.69	-0.21	196.33	-1.77	3.96	-0.08
	2050	22.45		69.48		194.57		3.88	

Figs. 7 to 10 depict the energy performance for the sixteen locations (sorted by latitude). The datasets were divided into subgroups according to the U-values pairs for opaque and transparent elements and their energy consumption results were averaged. In the figures, the left graphic depicts total energy consumption for air-conditioning (line with points) and cooling energy consumption (continuous blue line). The minimum energy consumption U-value subgroup is signaled with the diamond symbol. To the right, the graphic depicts the standard deviation (σ energy). The green curve indicates the baseline climate and the purple curve represents the 2050 climate projection.

The two graphics on the right side illustrate the difference in total energy consumption between the baseline and the 2050 climates (Δ energy) as well as the respective variation in cooling and heating energy consumption. The blue and red colors represent cooling and heating energy demand, respectively.

The left graphs of Figs. 7 to 10 indicate that as the U-value scale increases, total energy consumption also increases and cooling demand tends to stabilize both for current and future climate scenario. This behavior indicates that buildings with high U-values are more susceptible to winter conditions (more heating energy is required) while solar and internal gains do not dissipate as easily through the building's envelope with low U-values (more cooling energy is required). Total energy consumption also increases in all subgroups of the thermal transmittance scale for all locations, in relation to the baseline. The increase varies from 3 % in Istanbul (TUR) to 50 % in Malaga (ESP) in the subgroups with high U-values (Tel Aviv presents a 72 % rise in energy consumption, but for the reasons discussed above, it is not included in the overall comparison). A trend is observable in the increase of energy consumption as the latitude lowers to warmer regions. Except for Venice (ITA), Marseille (FRA), Istanbul (TUR), Naples (ITA), Algiers (DZA), and Casablanca (MAR), the difference in total energy consumption tends to rise as the U-values increase. In all of the locations and for all of the U-values subgroups, the increase in cooling demand is always greater than the decrease in heating energy consumption, as can be observed on the right-hand side of the figures. For high U-values, cooling demand may amount to a 137 % increase (Venice), while heating demand only decreases up to 63 % (Alexandria). The warming climate does not change the impact of the building geometry in the colder locations (higher latitudes), as the standard deviation (σ energy) values are very similar in both baseline and 2050 projection (second graph in Figs. 7 to 10); *e.g.*, Venice, Marseille, Podgorica, Istanbul, and Naples. However, in the remaining locations, the difference in the standard deviation between both cases tends to increase for higher U-values and has similar values in the lower U-values. This means that less insulated buildings (high U-values) in warmer future climates tend to be more affected by the choices of building geometry; *i.e.*, less robust. In the case of Alexandria, highly insulated buildings will even reduce the impact of the building geometry in comparison with the baseline climate.

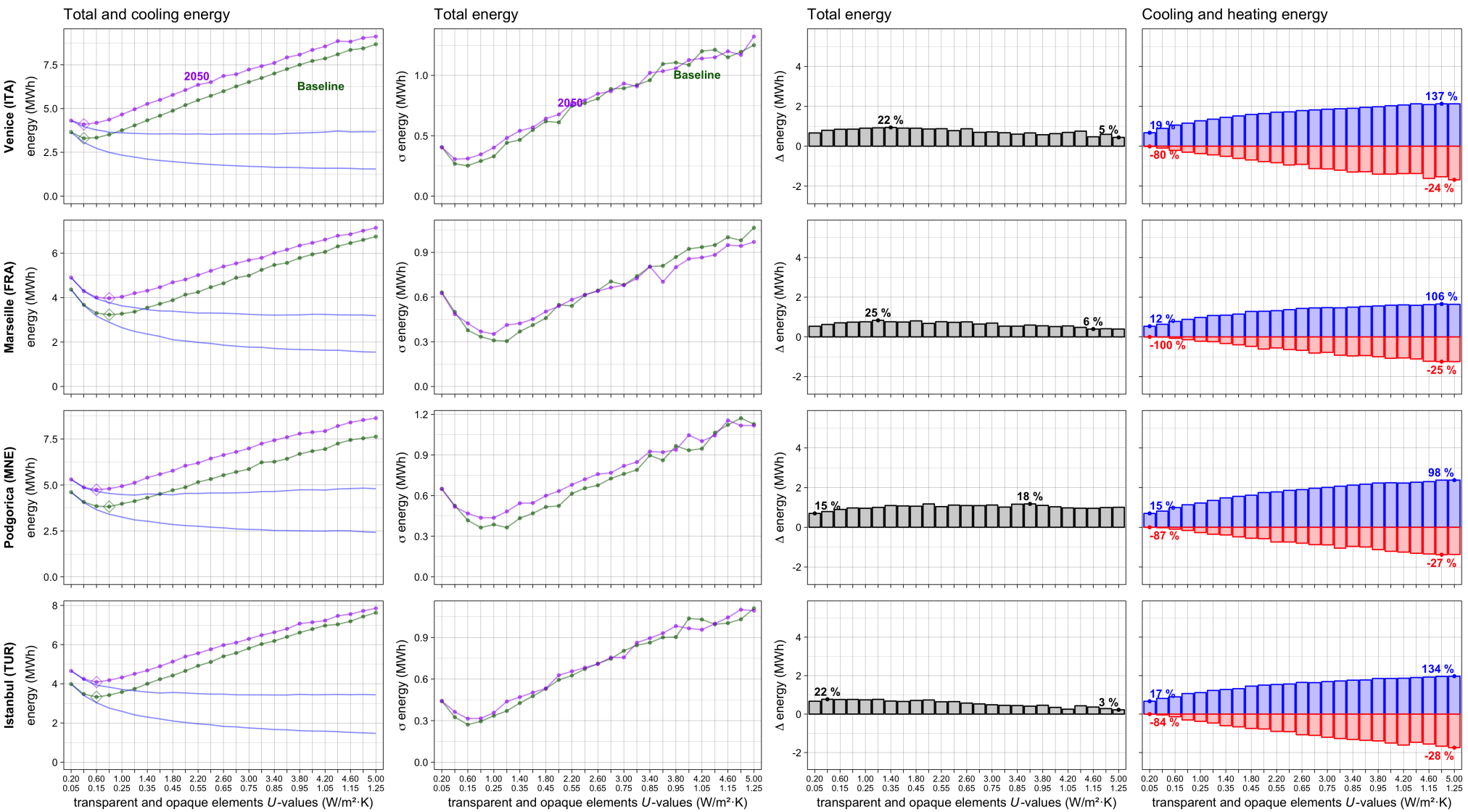

Fig. 7. Comparison between baseline weather and 2050 climate projection morphed weather data (part 1/4). The first and second graph column depict, respectively, the average total energy consumption (blue lines illustrate the cooling energy consumption) and the standard deviation (σ) for each subgroup of the 2050 climate projection and the baseline weather. The third and fourth graph columns present the difference in total energy consumption (Δ), and the difference in cooling (blue bars) and heating (red bars) energy consumption (Δ) between the 2050 climate projection and baseline weather, respectively.

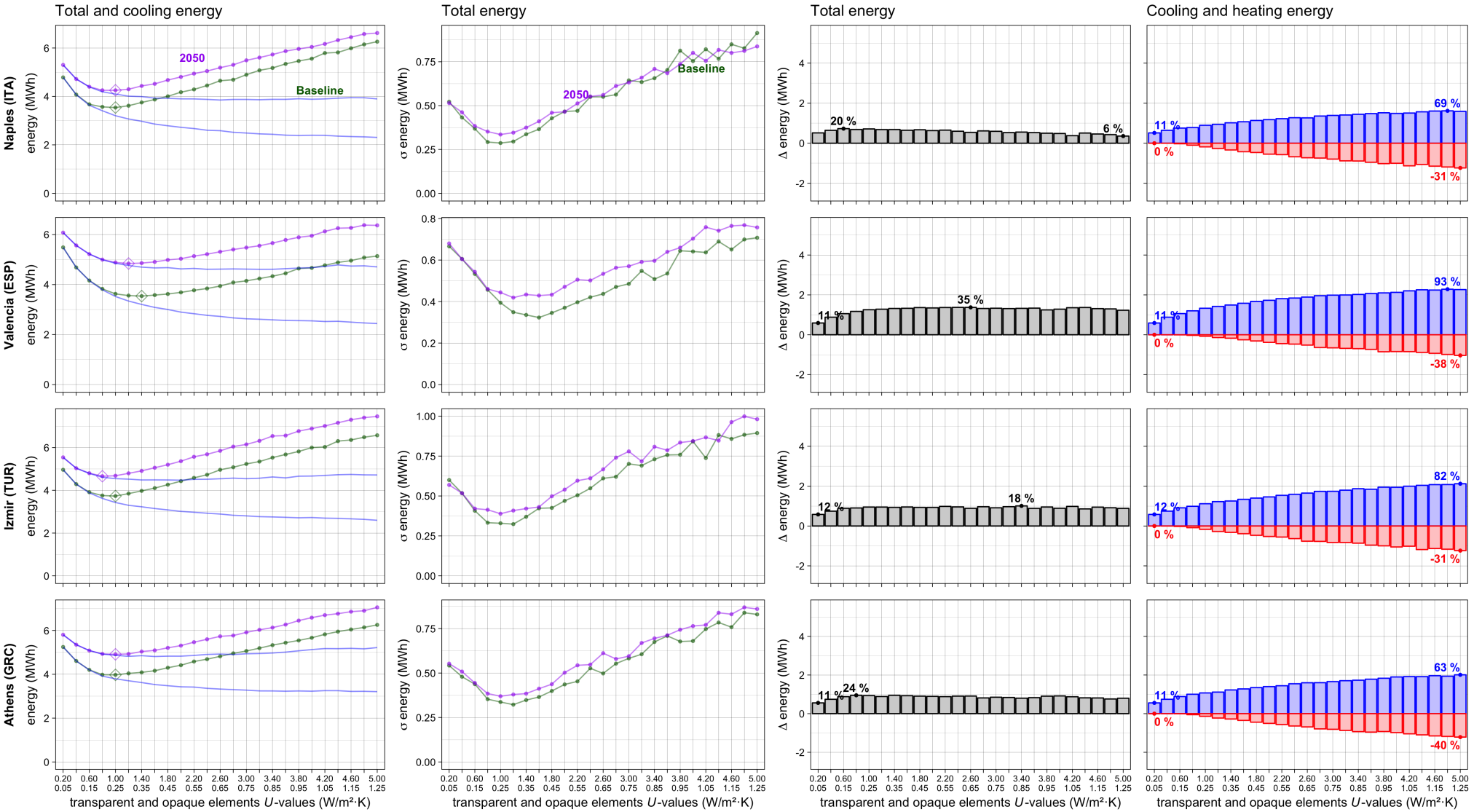

Fig. 8. Comparison between baseline weather and 2050 climate projection morphed weather data (part 2/4). The first and second graph column depict, respectively, the average total energy consumption (blue lines illustrate the cooling energy consumption) and the standard deviation (σ) for each subgroup of the 2050 climate projection and the baseline weather. The third and fourth graph columns present the difference in total energy consumption (Δ), and the difference in cooling (blue bars) and heating (red bars) energy consumption (Δ) between the 2050 climate projection and baseline weather, respectively.

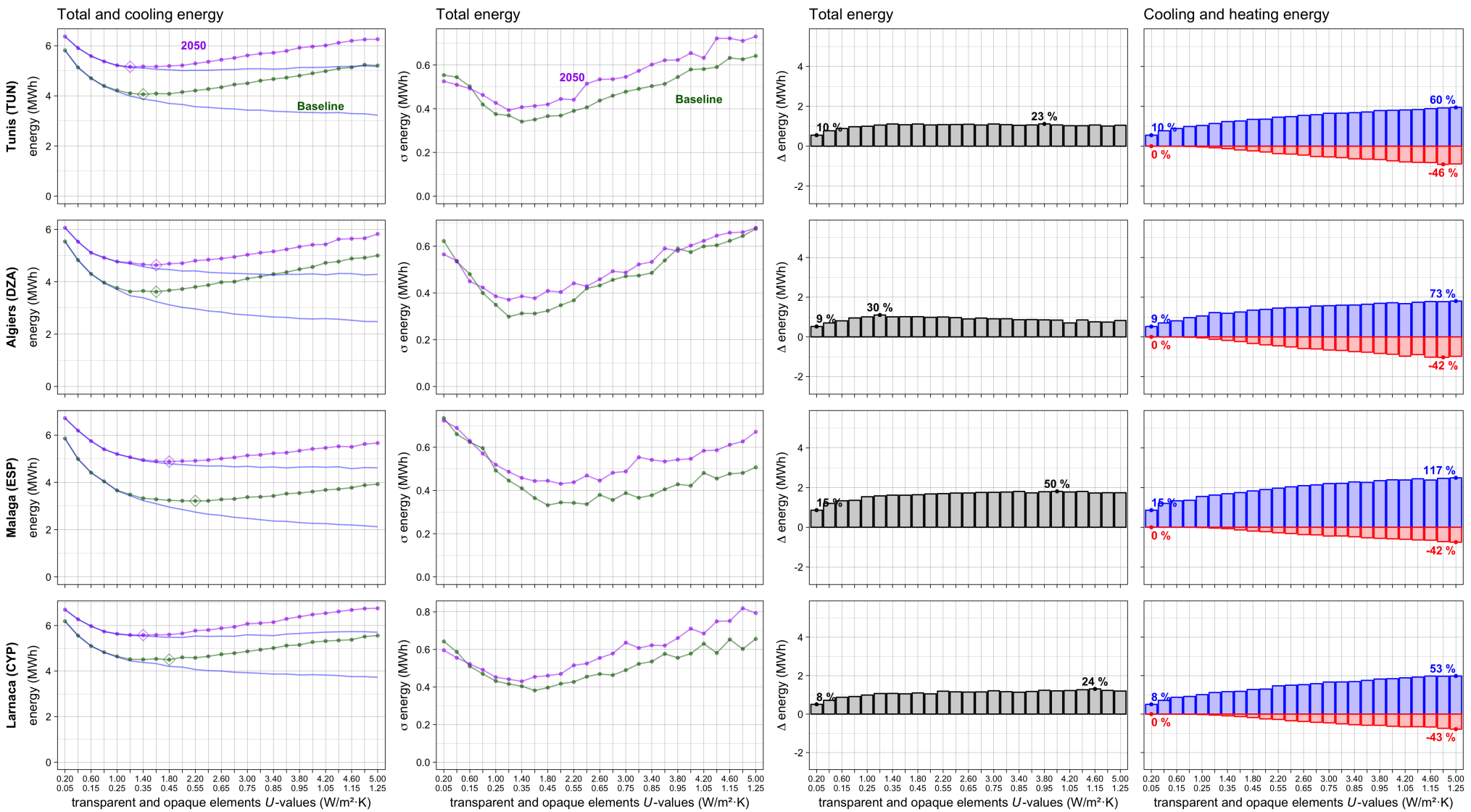

Fig. 9. Comparison between baseline weather and 2050 climate projection morphed weather data (part 3/4). The first and second graph column depict, respectively, the average total energy consumption (blue lines illustrate the cooling energy consumption) and the standard deviation (σ) for each subgroup of the 2050 climate projection and the baseline weather. The third and fourth graph columns present the difference in total energy consumption (Δ), and the difference in cooling (blue bars) and heating (red bars) energy consumption (Δ) between the 2050 climate projection and baseline weather, respectively.

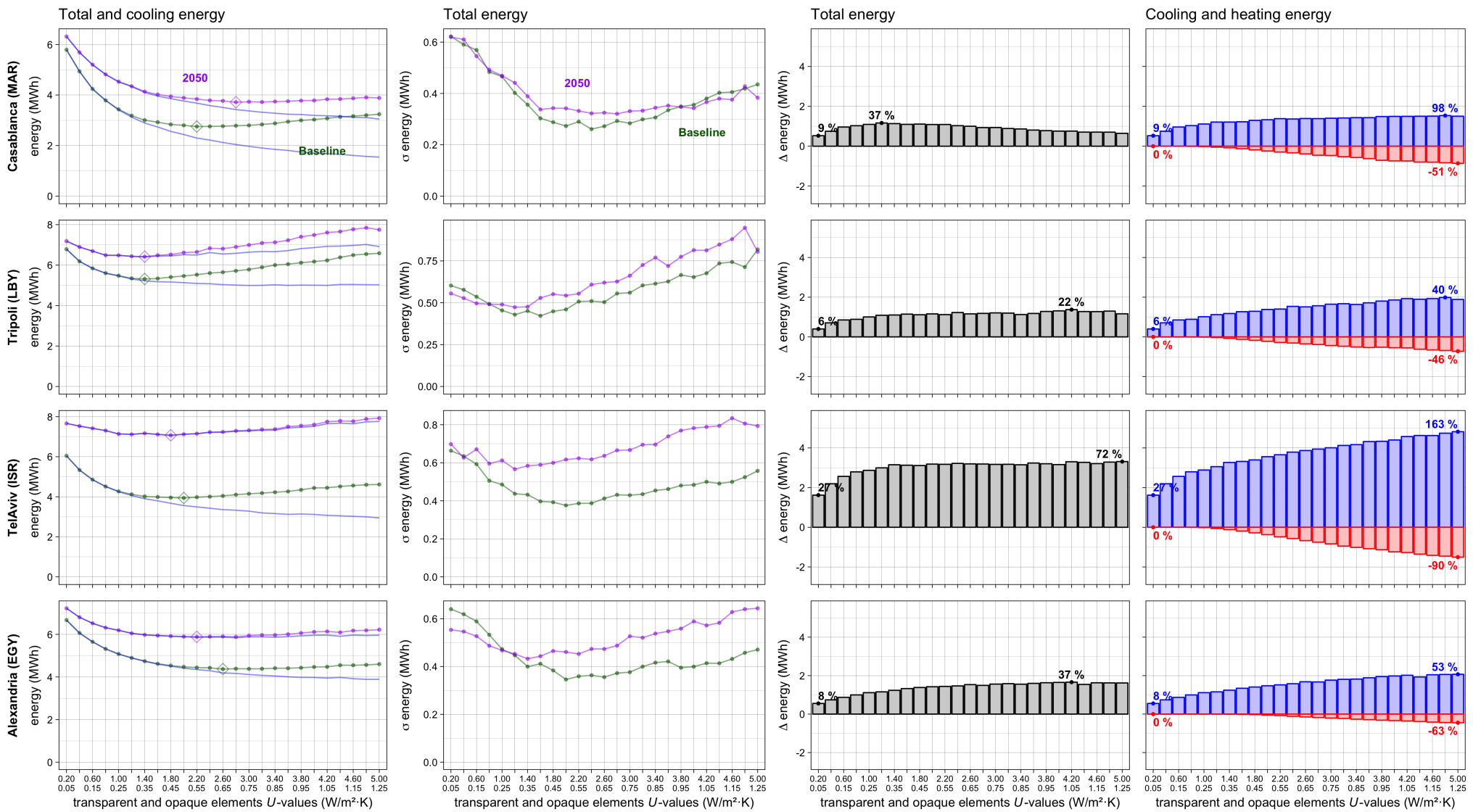

Fig. 10. Comparison between baseline weather and 2050 climate projection morphed weather data (part 4/4). The first and second graph column depict, respectively, the average total energy consumption (blue lines illustrate the cooling energy consumption) and the standard deviation (σ) for each subgroup of the 2050 climate projection and the baseline weather. The third and fourth graph columns present the difference in total energy consumption (Δ), and the difference in cooling (blue bars) and heating (red bars) energy consumption (Δ) between the 2050 climate projection and baseline weather, respectively.

Relatively to the main question of this study, the results show that buildings with ideal U-values for the baseline climate do not present any risk of overheating in the future. In fact, Malaga, Larnaca, and Alexandria even present significantly lower ideal U-values for the 2050 climate projection. Podgorica, Valencia, and Tunis only demonstrate a slight decrease in the ideal U-values. In these cases, the lower future ideal U-values mean that the increase in cooling energy consumption (in comparison to maintaining the higher ideal U-values of the baseline) is overcompensated by the reduction in heating energy consumption. The only exception is found for Casablanca, where the ideal U-values increase for the 2050 climate projection, thus leading to overheating if the ideal U-values of the baseline are used. In Venice, Podgorica, Izmir, Athens, Larnaca, Tripoli, Tel Aviv, and Alexandria cooling energy consumption increases significantly in the very low U-values and slightly in the high U-values; meaning that in the future in these locations, high U-values would lead to an increase in cooling energy consumption, contrarily to the current trend (baseline), where high U-values reduce, or at least do not increase cooling energy demand. Also noticeable is that in the most southern locations – Tripoli, Tel Aviv, and Alexandria – only the cooling energy consumption defines the ideal U-values for the 2050 climate projection. It should also be noted that ideal U-values were found for the averaged energy performance of the buildings of that subgroup, which does not mean that a particular building with its specific geometry and thermophysical properties would not behave differently and present its own risk of overheating. As weather data for the 2050 climate projection in Tel Aviv is from a more recent period, the presented results are overestimated. However, even these are in line with the main findings, which increases the confidence that these findings may resist under more severe climate change scenarios.

The main findings of this study can be summarized as follows:

- The impact of climate change tends to increase energy consumption more in the warmer climates of the Mediterranean.
- Buildings are less robust to global warming in hotter climates if they have higher U-values; *i.e.*, the buildings' energy performance is more prone to the choices in their geometry.
- Cooling energy consumption increases both for low and high U-values in Venice, Podgorica, Izmir, Athens, Larnaca, Tripoli, Tel Aviv, and Alexandria for the 2050 climate projection.
- Cooling energy consumption is the only factor to be considered in Tripoli, Tel Aviv, and Alexandria for the 2050 climate projection.
- The increase in cooling energy consumption will always be greater than the reduction of heating energy consumption in any choice of U-values.

- Except for Casablanca, the ideal U-values for the baseline climate will not increase the risk of overheating. In some cases (Malaga, Larnaca, and Alexandria), the ideal U-values in the 2050 climate projection have even smaller values. Podgorica, Valencia, and Tunis present a slight decrease in the ideal U-values.

4. Conclusion

The results clearly show a significant increase in cooling demands and a smaller reduction of heating energy consumption for the 2050 climate projection. This result is in line with findings in other studies that carry out a complete analysis of heating and cooling needs. As this study includes varying thermal transmittance values for the opaque and transparent elements, it was possible to determine the ideal U-values for each climate period for detached family houses. The comparison showed that ideal U-values do not increase for future climate projection, which indicates that current ideal U-values will not induce a risk of overheating (except for Casablanca). In fact, in several cases, the lowering of the thermal transmittance will be beneficial to reduce total energy consumption, despite being disadvantageous in todays' performance.

Therefore, the main conclusion of this paper is that two-story family houses, presenting the most adequate U-values for the baseline climate, will not suffer from overheating in the majority of the studied locations. Knowing if todays' highly insulated buildings will be prone to overheating is dependent on knowing what is the adequate amount and what can be considered as excessive. When buildings are over-insulated in today's climate, these will also probably be over-insulated in the future, thus suffering from overheating in both climate periods. Otherwise, the increase in cooling demands in the future cannot be attributed to having a low thermal transmittance envelope, thus other design strategies must be used to minimize the impact of the cooling demand, such as the use of shading devices, smaller windows and orientations with less solar-exposure, in particular during the summer season.

Finally, as Casablanca clearly falls outside of this general conclusion, further studies are required to find if this is either an outlier or there are other locations which may present similar results.

Data availability

The dataset related to the baseline weather for the sixteen locations in the Mediterranean can be found at URL `https://goo.gl/mfDXCd`, hosted at figshare [45]. The dataset related to the weather-morphed 2050 projection for the sixteen locations in the Mediterranean can be found at URL `https://bit.ly/2H9Y2cS`, hosted at figshare [46].

Acknowledgements

The research presented has been developed under the *Energy for Sustainability Initiative* of the University of Coimbra (UC). The authors are grateful to Adélio R. Gaspar for his valuable comments and insights. The authors are also thankful to Anabela Reis for proofreading the manuscript.

Funding: This work has been financed by the Portuguese Foundation for Science and Technology (FCT) and by the European Regional Development Fund (FEDER) through COMPETE 2020 – Operational Program for Competitiveness and Internationalization (POCI) in the framework of the research project Ren4EEnIEQ (PTDC/EMS-ENE/3238/2014, POCI-01-0145-FEDER-016760, and LISBOA-01-0145-FEDER-016760).

Declarations of interest: none.

References

[1] D. Dodman, Blaming cities for climate change? An analysis of urban greenhouse gas emissions inventories, Environment and Urbanization 21 (2009) 185–201. doi:10.1177/0956247809103016.

[2] E. S. Krayenhoff, M. Moustaoui, A. M. Broadbent, V. Gupta, M. Georgescu, Diurnal interaction between urban expansion, climate change and adaptation in US cities, Nature Climate Change 8 (2018) 1097–1103. doi:10.1038/s41558-018-0320-9.

[3] M. P. McCarthy, M. J. Best, R. A. Betts, Climate change in cities due to global warming and urban effects, Geophysical Research Letters 37 (2010) L09705. doi:10.1029/2010GL042845.

[4] M. Santamouris, On the energy impact of urban heat island and global warming on buildings, Energy and Buildings 82 (2014) 100–113. doi:10.1016/j.enbuild.2014.07.022.

[5] A. J. McMichael, R. E. Woodruff, S. Hales, Climate change and human health: Present and future risks, Lancet 367 (2006) 859–869. doi:10.1016/S0140-6736(06)68079-3.

[6] S. Vardoulakis, C. Dimitroulopoulou, J. Thornes, K. M. Lai, J. Taylor, I. Myers, C. Heaviside, A. Mavrogianni, C. Shrubsole, Z. Chalabi, M. Davies, P. Wilkinson, Impact of climate change on the domestic indoor environment and associated health risks in the UK, Environment International 85 (2015) 299–313. doi:10.1016/j.envint.2015.09.010.

[7] L. W. Davis, P. J. Gertler, Contribution of air conditioning adoption to future energy use under global warming, Proceedings of the National Academy of Sciences 112 (2015) 5962–5967. doi:10.1073/pnas.1423558112.

[8] Y. Petri, K. Caldeira, Impacts of global warming on residential heating and cooling degree-days in the United States, Scientific Reports 5 (2015) 12427. doi:10.1038/srep12427.

[9] D. H. Li, L. Yang, J. C. Lam, Impact of climate change on energy use in the built environment in different climate zones - A review, Energy 42 (2012) 103–112. doi:10.1016/j.energy.2012.03.044.

[10] M. Santamouris, C. Cartalis, A. Synnefa, D. Kolokotsa, On the impact of urban heat island and global warming on the power demand and electricity consumption of buildings—A review, Energy and Buildings 98 (2015) 119–124. doi:10.1016/j.enbuild.2014.09.052.

[11] F. Ascione, Energy conservation and renewable technologies for buildings to face the impact of the climate change and minimize the use of cooling, Solar Energy 154 (2017) 34–100. doi:10.1016/j.solener.2017.01.022.

[12] P. de Wilde, D. Coley, The implications of a changing climate for buildings, Building and Environment 55 (2012) 1–7. doi:10.1016/j.buildenv.2012.03.014.

[13] E. Rodrigues, M. S. Fernandes, A. R. Gaspar, Á. Gomes, J. J. Costa, Thermal transmittance effect on energy consumption of Mediterranean buildings with different thermal mass, Applied Energy 252 (2019) 113437. doi:10.1016/j.apenergy.2019.113437.

[14] Y. Zheng, Q. Weng, Modeling the effect of climate change on building energy demand in Los Angeles county by using a GIS-based high spatial- and temporal-resolution approach, Energy 176 (2019) 641–655. doi:10.1016/j.energy.2019.04.052.

[15] M. Herrera, S. Natarajan, D. A. Coley, T. Kershaw, A. P. Ramallo-González, M. Eames, D. Fosas, M. Wood, A review of current and future weather data for building simulation, Building Services Engineering Research and Technology 38 (2017) 602–627. doi:10.1177/0143624417705937.

[16] I. Andrić, M. Koc, S. G. Al-Ghamdi, A review of climate change implications for built environment: Impacts, mitigation measures and associated challenges in developed and developing countries, Journal of Cleaner Production 211 (2019) 83–102. doi:10.1016/j.jclepro.2018.11.128.

[17] A. Peacock, D. Jenkins, D. Kane, Investigating the potential of overheating in UK dwellings as a consequence of extant climate change, Energy Policy 38 (2010) 3277–3288. doi:10.1016/j.enpol.2010.01.021.

[18] D. Fosas, D. A. Coley, S. Natarajan, M. Herrera, M. Fosas de Pando, A. Ramallo-Gonzalez, Mitigation versus adaptation: Does insulating dwellings increase overheating risk?, Building and Environment 143 (2018) 740–759. doi:10.1016/j.buildenv.2018.07.033.

[19] I. G. Dino, C. M. Akgül, Impact of climate change on the existing residential building stock in Turkey: An analysis on energy use, greenhouse gas emissions and occupant comfort, Renewable Energy (2019). doi:10.1016/j.renene.2019.03.150.

[20] C. Cartalis, A. Synodinou, M. Proedrou, A. Tsangrassoulis, M. Santamouris, Modifications in energy demand in urban areas as a result of climate changes: an assessment for the southeast Mediterranean region, Energy Conversion and Management 42 (2001) 1647–1656. doi:10.1016/S0196-8904(00)00156-4.

[21] T. Zachariadis, P. Hadjinicolaou, The effect of climate change on electricity needs – A case study from Mediterranean Europe, Energy 76 (2014) 899–910. doi:10.1016/j.energy.2014.09.001.

[22] A. Moazami, V. M. Nik, S. Carlucci, S. Geving, Impacts of future weather data typology on building energy performance – Investigating long-term patterns of climate change and extreme weather conditions, Applied Energy 238 (2019) 696–720. doi:10.1016/j.apenergy.2019.01.085.

[23] M. Christenson, H. Manz, D. Gyalistras, Climate warming impact on degree-days and building energy demand in Switzerland, Energy Conversion and Management 47 (2006) 671–686. doi:10.1016/j.enconman.2005.06.009.

[24] T. Frank, Climate change impacts on building heating and cooling energy demand in Switzerland, Energy and Buildings 37 (2005) 1175–1185. doi:10.1016/j.enbuild.2005.06.019.

[25] L. Pajek, M. Košir, Implications of present and upcoming changes in bioclimatic potential for energy performance of residential buildings, Building and Environment 127 (2018) 157–172. doi:10.1016/j.buildenv.2017.10.040.

[26] I. Andrić, A. Pina, P. Ferrão, J. Fournier, B. Lacarrière, O. Le Corre, The impact of climate change on building heat demand in different climate types, Energy and Buildings 149 (2017) 225–234. doi:10.1016/j.enbuild.2017.05.047.

[27] I. Andrić, N. Gomes, A. Pina, P. Ferrão, J. Fournier, B. Lacarrière, O. Le Corre, Modeling the long-term effect of climate change on building heat demand: Case study on a district level, Energy and Buildings 126 (2016) 77–93. doi:10.1016/j.enbuild.2016.04.082.

[28] R. Barbosa, R. Vicente, R. Santos, Climate change and thermal comfort in Southern Europe housing: A case

study from Lisbon, Building and Environment 92 (2015) 440–451. doi:10.1016/j.buildenv.2015.05.019.

[29] S. Domínguez-Amarillo, J. Fernández-Agüera, J. J. Sendra, S. Roaf, The performance of Mediterranean low-income housing in scenarios involving climate change, Energy and Buildings (2019) 109374. doi:10.1016/j.enbuild.2019.109374.

[30] J. M. Rey-Hernández, C. Yousif, D. Gatt, E. Velasco-Gómez, J. San José-Alonso, F. J. Rey-Martínez, Modelling the long-term effect of climate change on a zero energy and carbon dioxide building through energy efficiency and renewables, Energy and Buildings 174 (2018) 85–96. doi:10.1016/j.enbuild.2018.06.006.

[31] V. Pérez-Andreu, C. Aparicio-Fernández, A. Martínez-Ibernón, J. L. Vivancos, Impact of climate change on heating and cooling energy demand in a residential building in a Mediterranean climate, Energy 165 (2018) 63–74. doi:10.1016/j.energy.2018.09.015.

[32] H. Campaniço, P. M. Soares, R. M. Cardoso, P. Hollmuller, Impact of climate change on building cooling potential of direct ventilation and evaporative cooling: a high resolution view for the Iberian Peninsula, Energy and Buildings (2019). doi:10.1016/j.enbuild.2019.03.017.

[33] Sustainable Energy Research Group, Energy and Climate Change Division, University of Southampton, Climate Change World Weather File Generator for World-Wide Weather Data – CCWorldWeatherGen, 2013. URL: http://www.energy.soton.ac.uk/ccworldweathergen/.

[34] E. Rodrigues, M. S. Fernandes, Á. Gomes, A. R. Gaspar, J. J. Costa, Performance-based design of multi-story buildings for a sustainable urban environment: A case study, Renewable and Sustainable Energy Reviews 113 (2019) 109243. doi:10.1016/j.rser.2019.109243.

[35] E. Rodrigues, A. R. Gaspar, Á. Gomes, Automated approach for design generation and thermal assessment of alternative floor plans, Energy and Buildings 81 (2014) 170–181. doi:10.1016/j.enbuild.2014.06.016.

[36] E. Rodrigues, A. R. Gaspar, Á. Gomes, Improving thermal performance of automatically generated floor plans using a geometric variable sequential optimization procedure, Applied Energy 132 (2014) 200–215. doi:10.1016/j.apenergy.2014.06.068.

[37] Energyplus, 2019. URL: https://energyplus.net.

[38] M. S. Fernandes, E. Rodrigues, A. R. Gaspar, J. J. Costa, Á. Gomes, The impact of thermal transmittance variation on building design in the Mediterranean region, Applied Energy 239 (2019) 581–597. doi:10.1016/j.apenergy.2019.01.239.

[39] M. Kottek, J. Grieser, C. Beck, B. Rudolf, F. Rubel, World Map of the Köppen-Geiger climate classification updated, Meteorologische Zeitschrift 15 (2006) 259–263. doi:10.1127/0941-2948/2006/0130.

[40] Climate.onebuilding.org, 2014. URL: http://climate.onebuilding.org/default.html.

[41] Intergovernmental Panel on Climate Change, United Nations, Data: Simulations, TAR (2001), SRES scenarios, HadCM3 Climate Scenario Data, 2001. URL: http://www.ipcc-data.org/sim/gcm_clim/SRES_TAR/hadcm3_download.html.

[42] M. F. Jentsch, A. B. S. Bahaj, P. A. James, Climate change future proofing of buildings-Generation and assessment of building simulation weather files, Energy and Buildings 40 (2008) 2148–2168. doi:10.1016/j.enbuild.2008.06.005.

[43] M. F. Jentsch, P. A. James, L. Bourikas, A. S. Bahaj, Transforming existing weather data for worldwide locations to enable energy and building performance simulation under future climates, Renewable Energy 55 (2013) 514–524. doi:10.1016/j.renene.2012.12.049.

[44] EnergyPlus Version 8.8 Documentation: Input Output Reference Manual, Technical Report, U.S. Department of Energy, 2017. URL: https://energyplus.net.

[45] E. Rodrigues, M. S. Fernandes, A. R. Gaspar, Á. Gomes, J. J. Costa, Dataset of high thermal inertia residential

buildings in sixteen mediterranean locations, 2018. URL: https://goo.gl/mfDXCd. doi:10.6084/m9.figshare.5732241.

[46] E. Rodrigues, M. S. Fernandes, Dataset of high thermal inertia residential buildings in sixteen mediterranean locations for the 2050 climate change projection, 2019. URL: https://bit.ly/2H9Y2cS. doi:10.6084/m9.figshare.8866253.